Direct simulation Monte Carlo for thin-film bearings

Francis J. Alexander, Alejandro L. Garcia,[a] and Berni J. Alder
Institute for Scientific Computing Research L-416, Lawrence Livermore National Laboratory, Livermore, California 94550

(Received 19 May 1994; accepted 17 August 1994)

The direct simulation Monte Carlo (DSMC) scheme is used to study the gas flow under a read/write head positioned nanometers above a moving disk drive platter (the slider bearing problem). In most cases, impressive agreement is found between the particle-based simulation and numerical solutions of the continuum hydrodynamic Reynolds equation which has been corrected for slip. However, at very high platter speeds the gas is far from equilibrium, and the load capacity for the slider bearing cannot be accurately computed from the hydrodynamic pressure. © *1994 American Institute of Physics.*

I. INTRODUCTION

Nanoscale design of computer components is no longer limited to chip technology but has recently been extended to mechanical devices as well. In a modern Winchester-type disk drive, the read/write head floats approximately 50 nm above the surface of the spinning platter.[1,2] Since this height is typically smaller than the mean-free path of molecules in the air (65 nm at STP), microscopic effects (slip length, gas–surface accommodation, surface roughness, etc.) are important.[3] The prediction of the vertical force on the head (as obtained from the pressure distribution in the gas) is a crucial design calculation since the head will not accurately read or write if it flies too high. If the head flies too low, it can catastrophically "crash" into the platter.

The head and platter together with the gas layer in between form a slider air bearing. Traditionally, macroscopic hydrodynamic equations (e.g., Navier–Stokes, Reynolds) have been used to model slider bearings.[4] The current trend toward nanoscale technology, however, is pushing the established limits of validity for these continuum descriptions.[5] The numerical study of microscopic flows necessitates either using simulations that model the fluid at the particle level or adding approximate corrections to macroscopic methods.

In the most basic particle method, molecular dynamics (MD) simulations, the trajectory of every particle in the fluid is computed from Newton's equations given an empirically determined interparticle potential.[6,7] Simple hydrodynamic phenomena, such as von Kármán vortex shedding[8] and Rayleigh–Bénard convection,[9] have been observed using molecular dynamics, however, MD simulations are not often used in fluid mechanics calculations because they are expensive in CPU time. Even with modern supercomputers, one typically simulates fewer than 10^6 particles over less than 10^{-9} s.

Fortunately, for a dilute gas there exist more efficient particle-based simulation algorithms. A popular method has been direct simulation Monte Carlo (DSMC), introduced by Bird in the early 1970s.[10,11] Whereas in molecular dynamics, one computes the *exact* trajectories of *all* the particles, DSMC uses a stochastic algorithm to evaluate collision probabilities and scattering distributions in accordance with kinetic theory. DSMC simulations typically run two to three *orders of magnitude* faster than MD codes, and state-of-the-art programs running on massively parallel computers can simulate complex flows with more than 10^8 particles over microseconds.

The DSMC method has been especially useful in aerospace engineering for computing flows of high Knudsen number (ratio of mean-free path to characteristic length).[12] The algorithm has been thoroughly tested over the past 20 years and found to be in excellent agreement with both experimental data[13,14] and molecular dynamics computations.[15,16] Recently, it was rigorously proved that DSMC is equivalent to a Monte Carlo solution of an equation "close" to the Boltzmann equation.[17] Finally, the DSMC method has been useful in the study of nonequilibrium fluctuations.[18]

In this paper, we present the results from DSMC simulations of the slider bearing problem and compare them with solutions to the slip-corrected Reynolds equation. Sections II and III briefly review the Reynolds equation formulation of the slider problem and the DSMC algorithm, respectively. In Sec. IV we compare the DSMC data and the Reynolds solutions in a variety of slider bearing scenarios. Finally, in Sec. V we discuss the future of particle simulations for this class of lubrication problems.

II. REYNOLDS EQUATION

Consider a channel formed by a stationary, slightly inclined surface above a horizontal surface, as illustrated in Fig. 1. The lower surface moves with velocity U in the x direction. A dilute gas occupies the space between the surfaces. The gas and the surfaces are assumed to be at a constant, ambient temperature, T_0. Since the incline is slight, typically less than 1°, the pressure in the gas p is taken to be constant in the vertical direction. At the left ($x=0$) and right ($x=L$) boundaries, the pressure in the gas is fixed at ambient pressure p_0.

The vertical force on the upper surface may be obtained from the load carrying capacity w, defined as

[a]Permanent address: Department of Physics, San Jose State University, San Jose, CA 95192-0106.

 1070-6631/94/6(12)/3854/7/$6.00

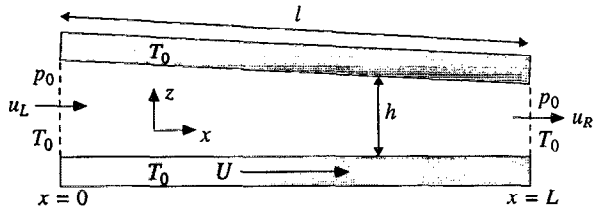

FIG. 1. Schematic of the slider bearing geometry.

$$w=\frac{1}{L}\int_0^L \frac{p(x)-p_0}{p_0}\,dx. \tag{1}$$

From standard lubrication theory,[4] the pressure in the gas may be computed from the Reynolds equation

$$\frac{d}{dx}\left(ph^3\frac{dp}{dx}\right)=6\mu U\frac{d}{dx}(ph), \tag{2}$$

where μ is the dynamic viscosity of the gas, and $h(x)$ is the vertical spacing between the walls; the minimum spacing is $h_0=h(x=L)$. It is more commonly solved in its nondimensional form,

$$\frac{d}{dX}\left(PH^3\frac{dP}{dX}\right)=\Lambda\frac{d}{dX}(PH), \tag{3}$$

where $X=x/l$, $P=p/p_0$, $H=h/h_0$, and the bearing number is defined as $\Lambda\equiv 6\mu Ul/p_0h_0^2$.

It was first pointed out by Maxwell that the velocity of a gas near a moving wall does not match the wall's velocity; this phenomenon is known as "velocity slip."[19,20] Specifically, the difference between the velocity of the wall and the velocity of the gas near the wall is $a\nabla_\perp\mathbf{u}$ where $\nabla_\perp\mathbf{u}$ is the velocity gradient normal to the wall. The slip length a is often approximated as being equal to λ, the mean-free path, which for a gas is

$$\lambda=\frac{\mu}{p}\sqrt{\frac{\pi RT_0}{2}}, \tag{4}$$

where R is the gas constant. However, this simple formulation for velocity slip is not accurate at a large Knudsen number.[15] If the wall is not fully accommodating (see Sec. III), then the slip length is

$$a=\sigma\frac{2-\alpha}{\alpha}\lambda, \tag{5}$$

where α is the accommodation coefficient, and the numerical factor $\sigma\simeq 1$.

A slip correction was first introduced into the Reynolds equation by Burgdorfer[21] as

$$\frac{d}{dX}\left(\left[1+\frac{12-6\alpha}{\alpha}\mathrm{Kn}\right]PH^3\frac{dP}{dX}\right)=\Lambda\frac{d}{dX}(PH), \tag{6}$$

where $\mathrm{Kn}=\lambda/h$ is the local Knudsen number. Fukui and Kaneko[22] developed a more sophisticated slip correction for the Reynolds equation,

$$\frac{d}{dX}\left[\bar{Q}_p(\mathrm{Kn})PH^3\frac{dP}{dX}\right]=\Lambda\frac{d}{dX}(PH). \tag{7}$$

The function $\bar{Q}_p(\mathrm{Kn})$ is the nondimensional flow rate for Poiseuille flow; a database of tabulated values for $\bar{Q}_p(\mathrm{Kn})$ is given in Ref. 23. For $\alpha=1$, Robert[24] gives the approximation

$$\bar{Q}_p(\mathrm{Kn})\simeq 1+6A\sqrt{\pi}\,\mathrm{Kn}+\frac{12}{\pi}\,\mathrm{Kn}\log(1+B\,\mathrm{Kn}), \tag{8}$$

where the parameters $A=1.318\,889$ and $B=0.387\,361$ are selected so as to give a best fit to the data in Ref. 23. The above expression for $\bar{Q}_p(\mathrm{Kn})$ is asymptotically correct as $\mathrm{Kn}\to\infty$ (free molecular limit) and as $\mathrm{Kn}\to 0$ (continuum limit).

Numerical solutions for the various forms of the Reynolds equation, Eqs. (3), (6), and (7), are presented in Sec. IV along with data from our DSMC simulations.

III. DSMC METHOD

In contrast with the macroscopic formulation presented in Sec. II, particle simulations model the fluid at the microscopic level. While the aerospace community is familiar with the direct simulation Monte Carlo (DSMC) algorithm, the method is not well known to researchers in lubrication theory. For this reason, we present a brief review of the algorithm; for a complete description see Refs. 10 and 11.

In the simulation, the state of the system is given by the positions and velocities of particles, $\{\mathbf{r}_i,\mathbf{v}_i\}$. Each particle in the simulation usually represents thousands of molecules in the physical system. In this sense, the DSMC method solves the Boltzmann equation using a representative random sample drawn from the actual velocity distribution. This rescaling allows us to model submicron systems using only 10^4–10^5 particles. However, if the number of particles in the simulation is too small, fewer than about 50 particles per cubic mean-free path, the DSMC method is not accurate.

The evolution of the system is integrated in time steps Δt. At each time step, the particles are moved as if they did not interact, i.e., their positions are updated to $\mathbf{r}_i+\mathbf{v}_i\Delta t$. Any particles that reach a boundary are processed according to the appropriate boundary condition. When all particles have been moved, a given number are selected for collisions. This splitting of the evolution between streaming and collisions is only accurate when the time step is a fraction of the mean collision time for a particle.

Our simulations employ two types of boundaries: thermal walls and fluxing reservoirs. The top and bottom edges in the simulation represent the read/write head and disk platter, respectively. When a particle strikes a fully accommodating thermal wall, the particle's velocity is reset according to a biased Maxwellian distribution. If the accommodation coefficient α is less than 1, then with probability α, the particle's velocity is thermalized by the wall and with probability $(1-\alpha)$ the particle is specularly reflected by the wall. For most gas–surface interactions, $\alpha\simeq 0.9$. More complicated accommodation schemes may also be used in DSMC.[25]

The left and right boundaries are treated as fluxing reservoirs, i.e., they act as infinite, equilibrium thermal baths at temperature T_0 and pressure p_0. The left and right reservoirs

have flow velocities u_L and u_R, respectively; how these velocities are set is described at the end of this section. At each time step, particles from the reservoirs flux into the system while particles already in the system can flux out.

To evaluate the collisions in the gas, the particles are sorted into cells whose sizes are typically a fraction of a cubic mean-free path. At each time step, particles within a cell are randomly selected as collision partners according to the collision probabilities derived from kinetic theory. In our simulations we use hard sphere collision rates with the scattering cross section of argon. For engineering applications, other types of collision rates are available to simulate other gases, such as air.[10]

Conservation of momentum and energy give four of the six equations needed to determine the post-collision velocities. The remaining two conditions are selected at random with the assumption that the direction of the post-collision relative velocity is uniformly distributed on the unit sphere. This assumption is valid for hard sphere particles at low densities and has been found to be an excellent approximation in general.[26]

Since DSMC is inherently a stochastic method, most physical quantities of interest are computed as time averages. The values of mass density $\hat{\rho}(\mathbf{r},t)$, momentum density $\hat{\mathbf{p}}(\mathbf{r},t)$, and energy density $\hat{e}(\mathbf{r},t)$ are periodically measured as

$$\begin{Bmatrix} \hat{\rho}(\mathbf{r},t) \\ \hat{\mathbf{p}}(\mathbf{r},t) \\ \hat{e}(\mathbf{r},t) \end{Bmatrix} = \sum_i \delta(\mathbf{r}_i - \mathbf{r}) \begin{Bmatrix} m \\ m\mathbf{v}_i \\ \frac{1}{2}m|\mathbf{v}_i|^2 \end{Bmatrix}, \tag{9}$$

where the caret indicates these are instantaneous, fluctuating values and m is the mass of a particle.[27] For steady flows, the fluid velocity is computed as $\mathbf{u}(\mathbf{r})=\mathbf{p}(\mathbf{r})/\rho(\mathbf{r})$ using the time averaged values of mass and momentum density. Temperature is computed from the equipartition theorem as

$$T(\mathbf{r}) = \frac{m}{3k} \frac{\langle \Sigma_i |\mathbf{v}_i - \mathbf{u}(\mathbf{r})|^2 \delta(\mathbf{r}_i - \mathbf{r}) \rangle}{\langle \Sigma_i \delta(\mathbf{r}_i - \mathbf{r}) \rangle} \tag{10}$$

or

$$T(\mathbf{r}) = \frac{2m}{3k} \left[\frac{e(\mathbf{r})}{\rho(\mathbf{r})} - \frac{1}{2} |\mathbf{u}(\mathbf{r})|^2 \right], \tag{11}$$

where the angle brackets denote time average and k is Boltzmann's constant.

Finally, the selection of the reservoir velocities u_L and u_R requires some care. In a real slider air bearing, a boundary layer develops near the inlet as the gas flows under the bearing.[4] A similar effect occurs at the trailing edge. This end effect is not present in the solution of the Reynolds equation since one assumes that the boundary layer is fully developed throughout the flow.

The sliders in our DSMC simulations are of finite length. When the reservoir velocities are set to U, the platter speed, the entrance and exit effects make comparison with Reynolds equation solutions impossible. Attempts at setting the reservoir velocities using theoretical calculations reduced, but did not remove the end effect. We solved this difficulty by monitoring the pressure in the first and last cells. The simulation adaptively changes the entrance and exit velocities so as to maintain ambient pressure at $x=0$ and $x=L$. This simple scheme allows us to mimic very long sliders using relatively small systems, as shown in Sec. IV.

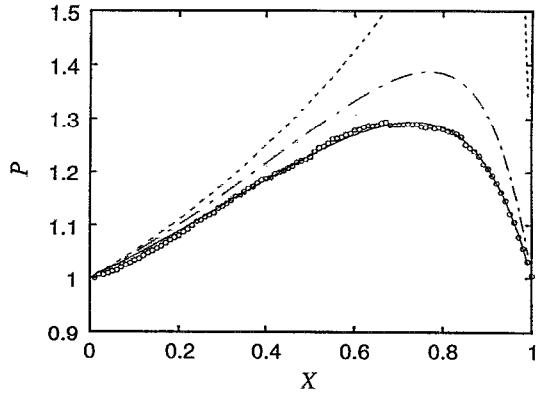

FIG. 2. Slider bearing pressure profile for $\mathrm{Kn}_0=1.250$, $\Lambda=61.6$, $\mathrm{Ma}=0.08$, and $\alpha=1.0$; solid line: Fukui and Kaneko; dot–dash line: first-order slip correction; dashed line: continuum; open circles: DSMC data.

IV. RESULTS

A number of different slider bearing configurations were studied using the DSMC method. The simulations used 8000–16 000 hard sphere particles with a diameter of 3.66 Å. For all runs, the ratio of the entrance to exit heights, $h(x=0)/h_0$, is fixed at two to one. The ambient pressure p_0 is atmospheric pressure, and the ambient temperature $T_0=273$ K. The mean-free path in the gas at ambient conditions is 62 nm. The viscosity of the gas is $\mu=2.08\times10^{-5}$ N s/m^2 and the sound speed is $c=307.8$ m/s. All the simulations were run on IBM RS6000 workstations.

To solve the Reynolds equation numerically, we replace the derivatives with their finite difference approximations. The resulting set of nonlinear equations are solved iteratively using Newton's method. For the Fukui–Kaneko correction, we use the Poiseuille flow rate given by Eq. (8) when $\alpha=1$ and the database in Ref. 23 when the accommodation coefficient is less than one.

For our first comparison, we consider a system of length $L=5$ μm with outlet height $h_0=50$ nm. The accommodation coefficient is unity ($\alpha=1$), so the walls are fully accommodating. The Knudsen number at the exit is $\mathrm{Kn}_0=\lambda/h_0=1.250$. The platter speed is $U=25$ m/s and the bearing number is $\Lambda=61.6$. Slider bearings in disk drives are typically longer, with $L\simeq1$ mm, giving a bearing number of $\Lambda\simeq10^3$–10^4. However, for the purpose of comparison with real slider bearings we consider the modified bearing number $\Lambda_b=\Lambda(b/l)^2$, where b is the width of the slider. For two-dimensional geometries, such as those treated in this paper, it is better to use Λ_b since it accounts for side flow in a finite width slider. For slider bearings used in disk drives, the ratio $b/l\simeq1/3$–$1/10$ and $\Lambda_b\simeq10$–10^3.

The solutions of the various Reynolds equations along with the pressure data from the DSMC simulation are presented in Fig. 2. The load capacity values are summarized in Table I. In the DSMC simulations, the load capacity w was

TABLE I. Summary of parameters and load capacities for various runs.

Knudsen number Kn_0	1.250	4.167	1.125	1.125
Bearing number Λ	61.6	1264	61.6	758
Accommodation α	1.0	1.0	0.7	1.0
Mach number $Ma=U/c$	0.08	0.5	0.08	1.0
Load capacity				
Continuum	0.365	0.383	0.365	0.383
First-order slip	0.229	0.369	0.153	0.378
Fukui and Kaneko	0.180	0.354	0.124	0.373
DSMC (from pressure)	0.175	0.357	0.129	0.370
DSMC (from force)	0.174	0.329	0.132	0.299

computed two ways: from the pressure distribution in the gas and from the momentum transfer of particles striking the upper wall. The continuum Reynolds equation without slip corrections compares poorly with DSMC. The pressure profile given by the first order slip-correction, Eq. (6), is in poor agreement with the DSMC data (about a 30% error in the load capacity). The agreement between the DSMC data and the Fukui–Kaneko modified Reynolds equation is good.

Next we consider a somewhat extreme scenario. In this second case, the length and height are reduced to $L=1.5$ μm and $h_0=15$ nm ($Kn_0=4.167$). We also increase the platter speed to $U=153.9$ m/s, i.e., half the sound speed. The bearing number for this system is $\Lambda=1264$. The Reynolds equation solutions and the particle simulation data are presented in Fig. 3 with the load capacities listed in Table I. The continuum solution of the Reynolds equation is in fair agreement despite the large Knudsen number because the bearing number is also high (when $\Lambda\to\infty$, $P\propto 1/H$). The first-order slip correction is in fair agreement and the Fukui–Kaneko solution is in good agreement with the DSMC data. Numerous other runs, with Knudsen numbers and bearing numbers between those considered in the two cases presented above, gave similar results.

For our third case, we return to our original parameters ($L=5$ μm, $h_0=50$ nm, and $U=25$ m/s) but reduce the accommodation to $\alpha=0.7$. The Reynolds equation solutions and the DSMC results are presented in Fig. 4; load capacities in Table I. As in Fig. 2, the pressure profile from the continuum (no-slip) Reynolds equation is too high. The first-order slip correction is in fair agreement with nearly a 20% error in the load capacity. However, the slip correction of Fukui and Kaneko is in good agreement with the DSMC data.

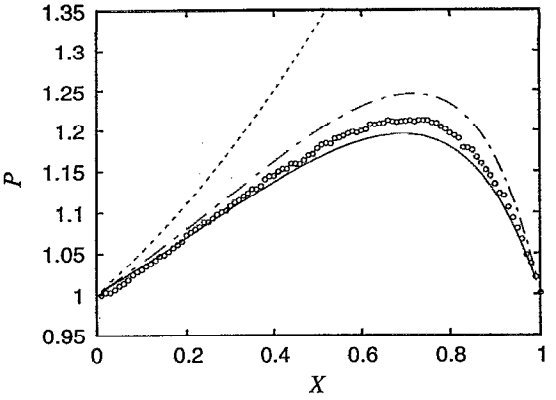

FIG. 4. Slider bearing pressure profile for $Kn_0=1.250$, $\Lambda=61.6$, $Ma=0.08$, and $\alpha=0.7$; symbols and line types as in Fig. 2.

The Reynolds equation is derived with the assumption that the Mach number $Ma=U/c$ is small, so it is interesting to test how well it does at high Mach number. We consider a system similar to our first case ($L=5$ μm, $h_0=50$ nm, and $\alpha=1.0$) but increase the platter speed to $U=307.8$ m/s so $Ma=1.0$. Figure 5 shows the pressure distributions computed from the Reynolds equation and measured in the DSMC simulation. All three Reynolds equation curves are in reasonable agreement with the DSMC pressure data since the bearing number is relatively high ($\Lambda=758$). However, looking at the load capacities listed in Table I, we discover an interesting discrepancy. The load capacity computed from the momentum transfer of particles striking the upper wall is significantly lower (more than 20%) than the load capacity obtained from the pressure distribution. If we increase the platter speed to $Ma=1.5$, the difference increases to nearly 40%.

To investigate this discrepancy in the load capacity, we consider a simpler geometry, specifically, planar Couette flow (see Fig. 6). The parameters in the Couette system are

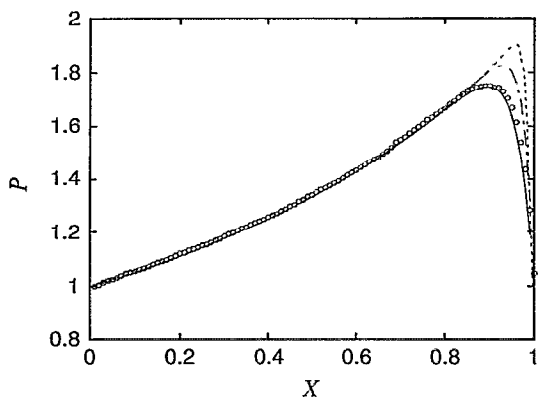

FIG. 3. Slider bearing pressure profile for $Kn_0=4.167$, $\Lambda=1264$, $Ma=0.50$, and $\alpha=1.0$; symbols and line types as in Fig. 2.

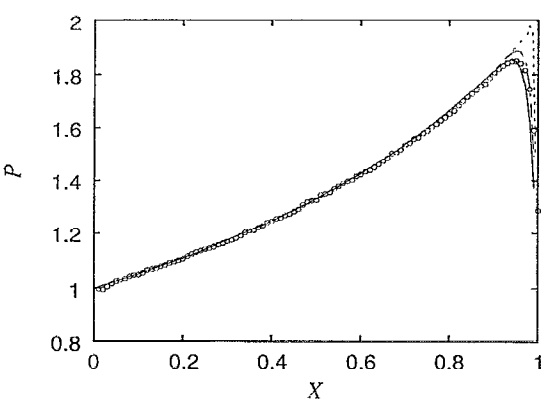

FIG. 5. Slider bearing pressure profile for $Kn_0=1.250$, $\Lambda=758$, $Ma=1.0$, and $\alpha=1.0$; symbols and line types as in Fig. 2.

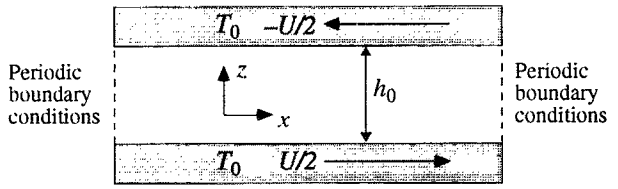

FIG. 6. Schematic of the Couette flow geometry.

similar to the slider bearing's ($L=5$ μm, $h_0=50$ nm, and $\alpha=1.0$). The wall's temperatures are fixed at $T_0=273$ K and at equilibrium, the pressure in the gas is 1 atm. The force on each wall is computed two ways: by measuring the time averaged change in the momentum of particles striking a wall and from the pressure in the gas computed using the ideal gas law. Clearly, the former is a direct measurement of the force while the latter is only correct so long as the gas remains in local equilibrium.[28] The load capacity, as determined via the two methods, as a function of Mach number is shown in Fig. 7. The load capacity increases with Mach number since the temperature (and consequently the pressure) increases due to viscous heating. However, there is a discrepancy between the two computations of load capacity and that difference increases with Mach number.

Given that the walls are less than a mean-free path apart, it should not be surprising that for high wall speeds (Ma >0.5) the gas is strongly out of equilibrium. Specifically, the velocity distribution for the particles is strongly non-Maxwellian. To illustrate this fact, we define the temperature components. T_x and T_z as the temperatures obtained using the equipartition theorem but only considering the x and z components of the particles' velocities, respectively. Figure 8 shows the temperature component profiles measured in the Couette flow system at various wall speeds. Clearly, at high Knudsen and Mach number, the stress tensor is anisotropic and thus the *average* pressure, as computed from the ideal gas law using the average temperature, will *not* give the correct force on the walls.[29]

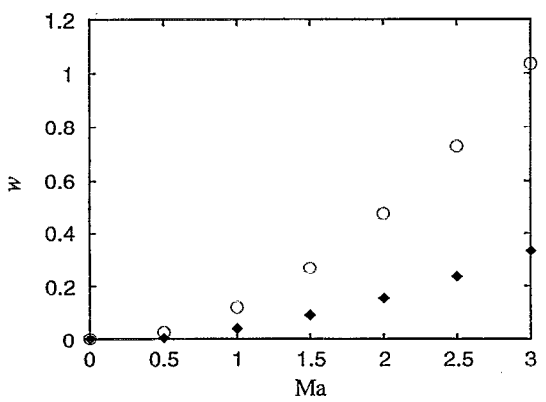

FIG. 7. Load capacity in planar Couette flow for $Kn_0=1.250$ and $\alpha=1.0$; open circles: computed from pressure in the gas; filled diamonds: computed from momentum transfer at the wall.

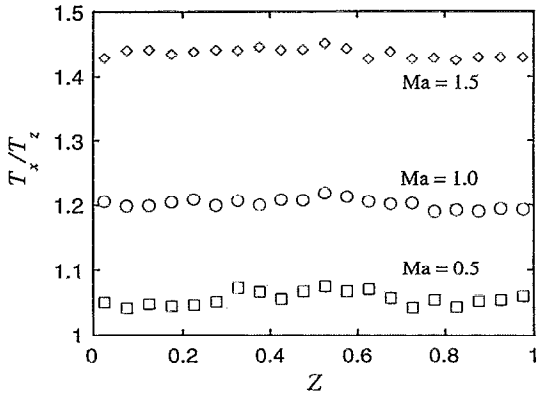

FIG. 8. Ratio of the temperature components T_x/T_z vs the vertical position $Z=z/h_0$ in planar Couette flow for $Kn_0=1.250$ and $\alpha=1.0$; squares: Ma $=0.5$; circles: Ma$=1.0$; diamonds: Ma$=1.5$.

As discussed in Sec. III, we carefully designed our inlet and outlet boundary conditions to eliminate end effects. Specifically, the inflow and outflow velocities, u_L and u_R, are adaptively adjusted so as to fix the pressure on each end to ambient pressure p_0. To illustrate the importance of these boundary conditions, consider a system with the same parameters as the slider bearing in Fig. 2. However, we now set $u_L=u_R=U$, i.e., the reservoir velocities are set equal to the platter velocity. Despite the fact that the reservoir pressure is fixed at p_0, Fig. 9 shows that the pressure distribution fails to match the boundary conditions and the measured load capacity ($w=0.270$) is more than 50% too large (compare with Fig. 2). Clearly, our comparisons between DSMC simulations and Reynolds equation solutions are only possible thanks to adaptive boundary conditions that eliminate this end effect.

Given the fact that the Knudsen number in our simulations is close to unity, one wonders if the flow is close to the free molecular limit. Since most of the computational effort in a DSMC simulation is in the calculation of interparticle collisions, our task would be greatly simplified if collisions were negligible. To test this conjecture, we ran a DSMC

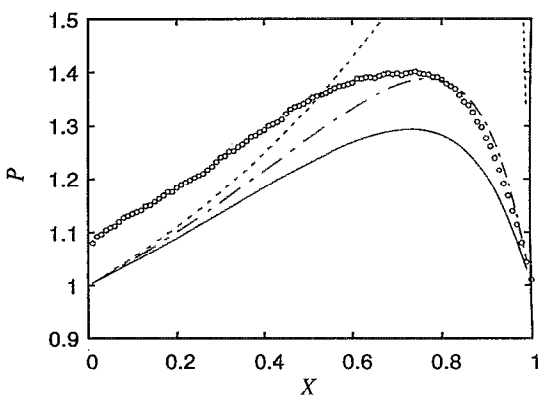

FIG. 9. Slider bearing pressure profile; parameters are the same as in Fig. 2 except the inlet and outlet velocities equal U, the platter velocity; symbols and line types as in Fig. 2.

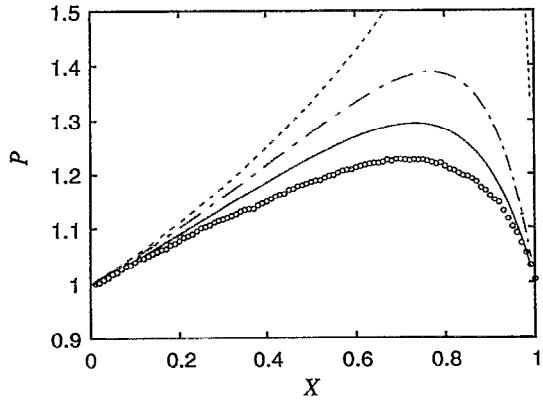

FIG. 10. Slider bearing pressure profile; parameters are the same as in Fig. 2 but with no collisions in the DSMC simulation (i.e., free molecular limit); symbols and line types as in Fig. 2.

simulation with the same parameters as in Fig. 2 but with the collisions subroutine disabled. The pressure profiles in Fig. 10 clearly show that collisions are not negligible, even when the slider height, h is on the order of a mean-free path. In the absence of collisions, the load capacity is significantly reduced ($w=0.142$) since the density (and consequently the pressure) of the gas is lower in the free molecular case.

V. CONCLUSIONS

This paper presents DSMC data for several slider bearing configurations and compares the results with various slip-corrected Reynolds equation solutions. Overall, the Fukui and Kaneko slip correction gave accurate results (see Figs. 2–4 and Table I), even in regimes where its validity was questionable. For very high platter speeds, anomalous load capacities were measured due to the breakdown of local equilibrium (see Figs. 7 and 8). Given the relative success of the slip-corrected Reynolds equation, one might question the need for microscopic, particle-based simulations of slider bearings.

In the study of nanoscale flows, DSMC simulations have several advantages over continuum hydrodynamic methods. First, the Reynolds equation assumes the flow has a fully developed boundary layer. Our boundary conditions were specifically designed to allow comparison with the Reynolds equation since the inlet and outlet flow velocities were adjusted so as to eliminate the boundary layer entrainment zone (see Fig. 9). Ideally, an air bearing simulation would not only include these regions but also the flow outside the slider. Preliminary attempts to use the Navier–Stokes equations for simulations of the entire slider plus the surrounding external flow have failed to span the large difference in length scales.[30] While it would be overly ambitious to attempt a simulation of the entire slider using DSMC, it is certainly feasible to perform detailed particle simulations of selected regions, such as the sections around the inlet or outlet.

Second, particle-based methods are especially useful in that microscopic parameters may be directly included in the simulation. For example, accommodation is an inherently atomic phenomenon. Experiments are underway to measure the distribution function $f(\mathbf{v}',\mathbf{v})$, where $\mathbf{v}$ is the velocity of a particle arriving at a surface and $\mathbf{v}'$ is its velocity leaving the surface, for disk drive platter surfaces.[31] This distribution function could be directly implemented in the subroutine that handles boundary reflections in a DSMC program. A related phenomenon is surface roughness; given the distribution of features, the surface topography can be directly included in a particle-based simulation. In macroscopic formulations, such as a Reynolds equation, surface effects can be included only by introducing *ad hoc* approximations; particle simulations are useful in testing and validating these phenomenological corrections.

Despite the many advantages in using DSMC for computing microscopic flows, particle methods remain costly since the sampling error goes as $O(\sqrt{1/N})$ where N is the number of computed time steps. In contrast, for most continuum fluid dynamics schemes, the truncation error is $O(\Delta t^2)$ so the error in the solution goes as $O(1/N^2)$. Given their computational expense, DSMC simulations are, at present, not competitive with slip-corrected Reynolds equations solvers as interactive design tools for air slider bearings. However, DSMC computations remain useful for testing and validating continuum hydrodynamic calculations at high Knudsen number. Similarly, for detailed studies of liquid thin-film lubrication, molecular dynamics simulations should prove increasingly useful.[32]

In the future, the DSMC method will be even more powerful when used in particle-continuum hybrid codes. These hybrids will use Navier–Stokes solvers for the low Knudsen number parts of the flow (e.g., exterior flow) and DSMC for the high Knudsen number areas of the flow (e.g., boundary layer).[33] At microscopic scales, the time step Δt used in DSMC simulations is the same as that used in Navier–Stokes computational fluid dynamics calculations.[34] Our group is currently developing a hybrid simulation with this capability for the study of various slider bearing geometries.

ACKNOWLEDGMENTS

The authors wish to acknowledge helpful discussions with F. F. Abraham, P. Alexopoulos, D. Baganoff, T. Denery, A. J. C. Ladd, G. McNamara, T. O'Sullivan, C. Rettner, L. Reyna, and J. Sobehart. This work was performed at Lawrence Livermore National Laboratory under the auspices of the Department of Energy under Contract No. W-7405-Eng-48. Numerical simulations were carried out at the OCF at LLNL.

[1] K. L. Deckert, "Computer-aided design of slider bearings in magnetic disk files," IBM. J. Res. Devel. **35**, 660 (1990).
[2] N. Tagawa, "State of the art for flying head slider mechanisms in magnetic recording disk storage," Wear **168**, 43 (1993).
[3] C. Cercignani, *Mathematical Methods in Kinetic Theory* (Plenum, New York, 1969); *The Boltzmann Equation and its Applications* (Springer, New York, 1988).
[4] W. A. Gross, L. A. Matsch, V. Castelli, A. Eshel, J. H. Vohr, and M. Wildmann, *Fluid Film Lubrication* (Wiley, New York, 1980).
[5] *Microscopic Simulation of Complex Flows*, edited by M. Mareschal, NATO ASI Series (Plenum, New York, 1990), Vol. 236; *Microscopic Simulations of Complex Hydrodynamic Phenomena*, edited by M. Mareschal and B. L. Holian, NATO ASI Series (Plenum, New York, 1992), Vol. 292.

[6]B. J. Alder and T. E. Wainwright, "Phase transition for a hard sphere system," J. Chem. Phys. **27**, 1208 (1957).
[7]M. P. Allen and D. J. Tildesley, *Computer Simulation of Liquids* (Clarendon, Oxford, 1987).
[8]L. Hannon, G. Lie, and E. Clementi, "Molecular dynamics simulation of flow past a plate," J. Sci. Comput. **1**, 145 (1986); E. Meiburg, "Comparison of the molecular dynamics method and the direct simulation Monte Carlo technique for flows around simple geometries," Phys. Fluids **29**, 3107 (1986); D. C. Rapaport and E. Clementi, "Eddy formation in obstructed fluid flows: A molecular dynamics study," Phys. Rev. Lett. **57**, 695 (1987).
[9]M. Mareschal and E. Kestemont, "Experimental evidence for convective rolls in finite two-dimensional molecular models," Nature **329**, 427 (1987); M. Mareschal and E. Kestemont, "Order and fluctuations in nonequilibrium molecular dynamics simulations of two-dimensional fluids," J. Stat. Phys. **48**, 1187 (1987); D. C. Rapaport, "Molecular dynamics study of Rayleigh–Bénard convection," Phys. Rev. Lett. **60**, 2480 (1988); M. Mareschal, M. Malek Mansour, A. Puhl, and E. Kestemont, "Molecular dynamics vs hydrodynamics in a two-dimensional Rayleigh–Bénard system," *ibid.* **61**, 2550 (1988).
[10]G. A. Bird, *Molecular Gas Dynamics* (Clarendon, Oxford, 1976); *Molecular Gas Dynamics and the Direct Simulation of Gas Flows* (Clarendon, Oxford, 1994).
[11]A. L. Garcia, *Numerical Methods for Physics* (Prentice–Hall, Englewood Cliffs, NJ, 1994), Chap. 10.
[12]E. P. Muntz, "Rarefied gas dynamics," Annu. Rev. Fluid Mech. **21**, 387 (1989).
[13]D. A. Erwin, G. C. Pham-Van-Diep, and E. P. Muntz, "Nonequilibrium gas flows. I. A detailed validation of Monte Carlo direct simulation for monatomic gases," Phys. Fluids A **3**, 697 (1991).
[14]D. C. Wadsworth, "Slip effects in a confined rarefied gas. I. Temperature slip," Phys. Fluids A **5**, 1831 (1993).
[15]D. L. Morris, L. Hannon, and A. L. Garcia, "Slip length in a dilute gas," Phys. Rev. A **46**, 5279 (1992).
[16]E. Salomons and M. Mareschal, "Usefulness of the Burnett description of strong shock waves," Phys. Rev. Lett. **69**, 269 (1992).
[17]W. Wagner, "A convergence proof for Bird's direct simulation Monte Carlo method for the Boltzmann equation," J. Stat. Phys. **66**, 1011 (1992).
[18]M. Malek Mansour, A. L. Garcia, G. C. Lie, and E. Clementi, "Fluctuating hydrodynamics in a dilute gas," Phys. Rev. Lett. **58**, 874 (1987).
[19]J. C. Maxwell, "On stresses in rarefied gases arising from inequalities of temperature," Philos. Trans. R. Soc. London **170**, 231 (1867); W. G. Vincenti and C. H. Kruger, *Introduction to Physical Gas Dynamics* (Krieger, Malabar, FL, 1965).
[20]A similar effect for temperature is called "temperature jump."
[21]A. Burgdorfer, "The influence of the molecular mean-free path on the performance of hydrodynamic gas lubricated bearings," Trans. ASME **81**, 94 (1959).
[22]S. Fukui and R. Kaneko, "Analysis of ultrathin gas film lubrication based on linearized Boltzmann equation: First report derivation of a generalized lubrication equation including thermal creep flow," J. Tribology **110**, 253 (1988).
[23]S. Fukui and R. Kaneko, "A database for interpolation of Poiseuille flow rates for high Knudsen number lubrication problems," J. Tribology **112**, 78 (1990).
[24]M. Robert (personal communication).
[25]R. G. Lord, "Direct simulation Monte Carlo calculations of rarefied flows with incomplete surface accommodation," J. Fluid Mech. **239**, 449 (1992).
[26]G. A. Bird, "A contemporary implementation of the direct simulation Monte Carlo method," in *Microscopic Simulations of Complex Hydrodynamic Phenomena*, edited by M. Mareschal and B. L. Holian, NATO ASI Series (Plenum, New York, 1992), Vol. 292.
[27]In the simulation, these densities are not computed at a point $\mathbf{r}$ but rather in a cell (of volume V_s) about the point $\mathbf{r}$. The sum is then restricted to particles within this volume and the Dirac delta is replaced by $1/V_s$.
[28]J. A. McLennan, *Introduction to Nonequilibrium Statistical Mechanics* (Prentice–Hall, Englewood Cliffs, NJ, 1989).
[29]A fluid system does not necessarily need to be out of equilibrium to exhibit anisotropies in the normal components of the stress tensor. For example, due to surface tension, these components can be different at an interface.
[30]W. D. Henshaw, L. G. Reyna, and J. A. Zufiria, "Compressible Navier–Stokes computations for slider air bearings," J. Tribology **113**, 73 (1991).
[31]C. Rettner (personal communication).
[32]M. O. Robbins, P. A. Thompson, and G. S. Grest, "Simulations of nanometer-thick lubricating films," MRS Bull. **18**, 45 (1993).
[33]D. C. Wadsworth and D. A. Erwin, "One-dimensional hybrid continuum/particle simulation approach for rarefied hypersonic flows," AIAA Paper No. AIAA-90-1690, 1990.
[34]In a Navier–Stokes solver, for a grid size of a mean-free path, the Courant–Friedrichs–Lewy stability condition requires that $\Delta t \leq \lambda/c$, i.e., roughly less than or equal to the mean collision time for a particle.